Check for updates

ChemSusChem

Research Article
doi.org/10.1002/cssc.202301063

Chemistry Europe
European Chemical Societies Publishing

www.chemsuschem.org

Investigating the Influence of Treatments on Carbon Felts for Vanadium Redox Flow Batteries

Monja Schilling,[b] László Eifert,[b] Kerstin Köble,[b] Maximilian Jaugstetter,[c] Nico Bevilacqua,[b] Kieran F. Fahy,[d] Kristina Tschulik,[c] Aimy Bazylak,[d] and Roswitha Zeis*[a, b, d]

Vanadium redox flow battery (VRFB) electrodes face challenges related to their long-term operation. We investigated different electrode treatments mimicking the aging processes during operation, including thermal activation, aging, soaking, and storing. Several characterization techniques were used to deepen the understanding of the treatment of carbon felts. Synchrotron X-ray imaging, electrochemical impedance spectroscopy (EIS) with the distribution of relaxation times analysis, and dynamic vapor sorption (DVS) revealed differences between the wettability of felts. The bulk saturation after electrolyte injection into the carbon felts significantly differed from 8% to 96%. DVS revealed differences in the sorption/desorption behavior of carbon felt ranging from a slight change of 0.8 wt% to over 100 wt%. Additionally, the interactions between the water vapor and the sample change from type V to type H2. After treatment, morphology changes were observed by atomic force microscopy and scanning electron microscopy. Cyclic voltammetry and EIS were used to probe the electrochemical performance, revealing different catalytic activities and transport-related impedances for the treated samples. These investigations are crucial for understanding the effects of treatments on the performance and optimizing materials for long-term operation.

Introduction

The Vanadium Redox Flow Battery (VRFB) is a promising candidate for large-scale energy storage and can help to store energy from renewable sources while balancing fluctuations in the electrical grid. Nevertheless, this already commercially available technology must overcome major challenges to enhance the battery's efficiency and long-term operation. Crucial parts of VRFBs are the electrodes, which should exhibit high catalytic activity and corrosion resistance in harsh conditions to achieve long lifetimes.[1,2] Usually, carbon-based materials such as carbon felt, carbon paper, or carbon cloth are used as VRFB electrodes. Since these materials show a low activity towards the vanadium redox reactions and poor wettability, it is common to pretreat them before the cell assembly. A typical activation process is based on the thermal activation of carbon-based materials to enhance their performance by oxidizing the surface.[3–5] Since VRFBs are developed for long-term use, investigating aging effects is crucial. Eifert et al.[5–7] characterized carbon felt materials after different aging treatments using different methods, such as differential electrochemical mass spectroscopy, X-ray photoelectron spectroscopy, and cyclic voltammetry. They identified the carbon corrosion in the positive half-cell and the Hydrogen Evolution Reaction (HER) in the negative half-cell as the dominating side reactions. The parasitic HER, which takes place in the same potential range as the vanadium(III)/vanadium(II) reaction, was investigated by many research groups worldwide.[8–13] In these works, different methods to prevent the reaction are discussed including metal- or carbon-based nanomaterials as additives[13] introducing bismuth[8,9] or electron-deficient sites,[12] or using appropriate carbon fiber material.[10] Nevertheless, the perfect solution was still not found; therefore, the VRFB's performance still suffers from this undesired HER starting at an already low State of Charge (SoC)[14] and material degradation due to carbon corrosion of the electrode and bipolar plate[1] shortening the lifetime and efficiency of the battery. Carbon corrosion especially takes place at high applied potentials in the positive half-cell.[6,7] Besides decreasing the efficiency of this particular cycle since electrons are utilized for the carbon corrosion reaction instead of the V(IV) oxidation, the performance of the battery is decreased for all further cycles due to the loss of catalytic active carbon material. In the worst case, the carbon

[a] Prof. Dr. R. Zeis
Faculty of Engineering, Department of Electrical, Electronics, and Communication Engineering
Friedrich-Alexander-Universität Erlangen-Nürnberg (FAU)
Cauerstraße 9, 91058 Erlangen (Germany)
E-mail: roswitha.zeis@fau.de

[b] M. Schilling, Dr. L. Eifert, K. Köble, Dr. N. Bevilacqua, Prof. Dr. R. Zeis
Helmholtz Institute Ulm
Karlsruhe Institute of Technology
Helmholtzstraße 11, 89081 Ulm (Germany)

[c] Dr. M. Jaugstetter, Prof. Dr. K. Tschulik
Faculty of Chemistry and Biochemistry, Analytical Chemistry II
Ruhr University Bochum
Universitätsstraße 150, 44801 Bochum (Germany)

[d] Dr. K. F. Fahy, Prof. Dr. A. Bazylak, Prof. Dr. R. Zeis
Faculty of Applied Science & Engineering, Department of Mechanical & Industrial Engineering
University of Toronto
5 King's College Road, Toronto, Ontario, M5S 3G8 (Canada)

Supporting information for this article is available on the WWW under https://doi.org/10.1002/cssc.202301063

© 2023 The Authors. ChemSusChem published by Wiley-VCH GmbH. This is an open access article under the terms of the Creative Commons Attribution Non-Commercial License, which permits use, distribution and reproduction in any medium, provided the original work is properly cited and is not used for commercial purposes.

© 2023 The Authors. ChemSusChem published by Wiley-VCH GmbH

material in the cell stack must be renewed to improve the performance.

In addition to the problems related to side reactions, a fully saturated electrode is crucial for achieving excellent performance since the material surface must be wetted to serve as an active site for the chemical reaction. Furthermore, the flow behavior of the electrolyte through the electrode should be investigated to limit pumping losses and optimize the mass transport of the electroactive species.[1,15] The wettability of the material will crucially affect all of these issues.

In recent years, (synchrotron) X-ray imaging has become a vital technique to visualize the electrolyte flow behavior in the electrode.[15–17,18] Our group investigated the impact of the compression rate and the electrolyte species on the electrolyte invasion and the flow behavior within the electrode structure.[15–17] Here, wettability plays a vital role in achieving high electrolyte saturations. Other approaches are needed since experiments at a synchrotron facility are often complex, time-consuming, costly, and have limited access. In our previous study, we demonstrated that Electrochemical Impedance Spectroscopy (EIS) coupled with the Distribution of Relaxation Times (DRT) analysis is suitable to study processes in the VRFB's electrode. We were able to identify processes in the different frequency ranges including the electrochemical reaction and different transport-related processes. This knowledge is crucial in understanding the processes in the electrode and can be used to optimize this part of the battery.[19] Combined with Dynamic Vapor Sorption (DVS) measurements, the DRT spectrum reveals essential information regarding electrode wettability and morphology.[20] To date, there are studies available investigating the aging mechanisms in VRFBs. However, there is a scarcity of studies that reveal the influences of these aging mechanisms on all the important parameters for flow battery operation, namely the structure, the wettability, and the electrochemical performance of the electrode material.

This study investigates how different treatments, including thermal activation and subsequent aging, soaking in sulfuric acid, or storing, impact carbon felt properties. These electrode treatments represent typical aging processes occurring in VRFBs. The impact of these treatments is investigated using different characterization methods. Synchrotron X-ray imaging, DVS, EIS, and DRT analysis were applied to assess wettability and flow behavior. The electrochemical performance of the materials was thoroughly characterized with Cyclic Voltammetry (CV), investigating the reactions in both half-cell reactions. Since the carbon felts undergo structural changes at the surface during treatment, Atomic Force Microscopy (AFM) and Scanning Electron Microscopy (SEM) were used to examine the surface morphology.

Results and Discussion

This section will highlight the influence of wettability on synchrotron X-ray imaging experiments, EIS, and DVS measurements. Furthermore, the relationship between morphology and electrochemical performance will be shown by SEM, AFM, and CV studies.

Structural Analysis by AFM and SEM

This section will discuss treatments' influence on the carbon felts' morphology. The structural changes were investigated using SEM and AFM. Several fibers of each sample were probed during the measurements, and representative images were selected for this publication (Figure 1). Generally, the studied carbon felt surface (all samples fabricated from one batch of material) is inhomogeneous, displaying many kinks and edges. The carbon fibers comprise several bundled rods, as reported in the literature.[5,20,21]

In a previous publication of our group,[20] a thermal activation process of the carbon felt at 400 °C for 25 h in the air was identified as optimum regarding increased wettability, increased pore formation, and therefore, higher surface area, and less weight loss of the material during the thermal activation step. Here, we used the same conditions for the activation step. The activated carbon felt shows a rough surface with nano-sized holes (Figures 1a and b). To study the effect of VRFB operation, a thermally activated carbon felt was electrochemically aged by applying a potential of 1.2 V vs. RHE for 5 days while soaking the electrode in the vanadium-containing electrolyte. This harsh treatment reflects the conditions in the positive half-cell at high SoC.[7] In this potential range, carbon corrosion will occur.[6,7] After the aging treatment, the felt's surface is more smooth compared to the activated carbon felt. The overall structure of the fibers, the bundled rods is similar for both materials and is still intact, proving that the aging treatment only influenced the surface of the fiber and did not lead to a drastic loss of most parts of the fiber. Thus, the small nano-sized pores are still visible in the SEM image (Figure 1c), but the fiber surface is smoother according to the AFM analysis (Figure 1d). Since the surface of the carbon fiber is inhomogeneous, the potential distribution at the fiber's surface will not be homogeneous either. The carbon corrosion will most likely occur at the structure's kinks and edges, including the nano-structured holes since kinks and edges lead to potential spikes fostering this reaction.[22] Additionally, the acidic environment alters the surface, including the functional groups.[5] This effect is also visible in the SEM and AFM images of the carbon felt soaked in sulfuric acid (Figures 1e and f), whose fiber generally displays a smoother surface than the original activated sample. The surface of the stored carbon felt is less roughed than the (freshly) activated carbon felt (Figures 1g and h). Thus, the effect of storing (under ambient air conditions) is not neglectable for the material's structure and performance, as also demonstrated in the following chapters. The aged, soaked, and stored carbon felts all display small, spherical particles on top of the surface. They are most likely impurities such as adventitious carbon and are obtained from the manufacturing process and the exposure of the sample to air.

© 2023 The Authors. ChemSusChem published by Wiley-VCH GmbH

1864564x, 2024, 1, Downloaded from https://chemistry-europe.onlinelibrary.wiley.com/doi/10.1002/cssc.202301063, Wiley Online Library on [01/08/2024]. See the Terms and Conditions (https://onlinelibrary.wiley.com/terms-and-conditions) on Wiley Online Library for rules of use; OA articles are governed by the applicable Creative Commons License

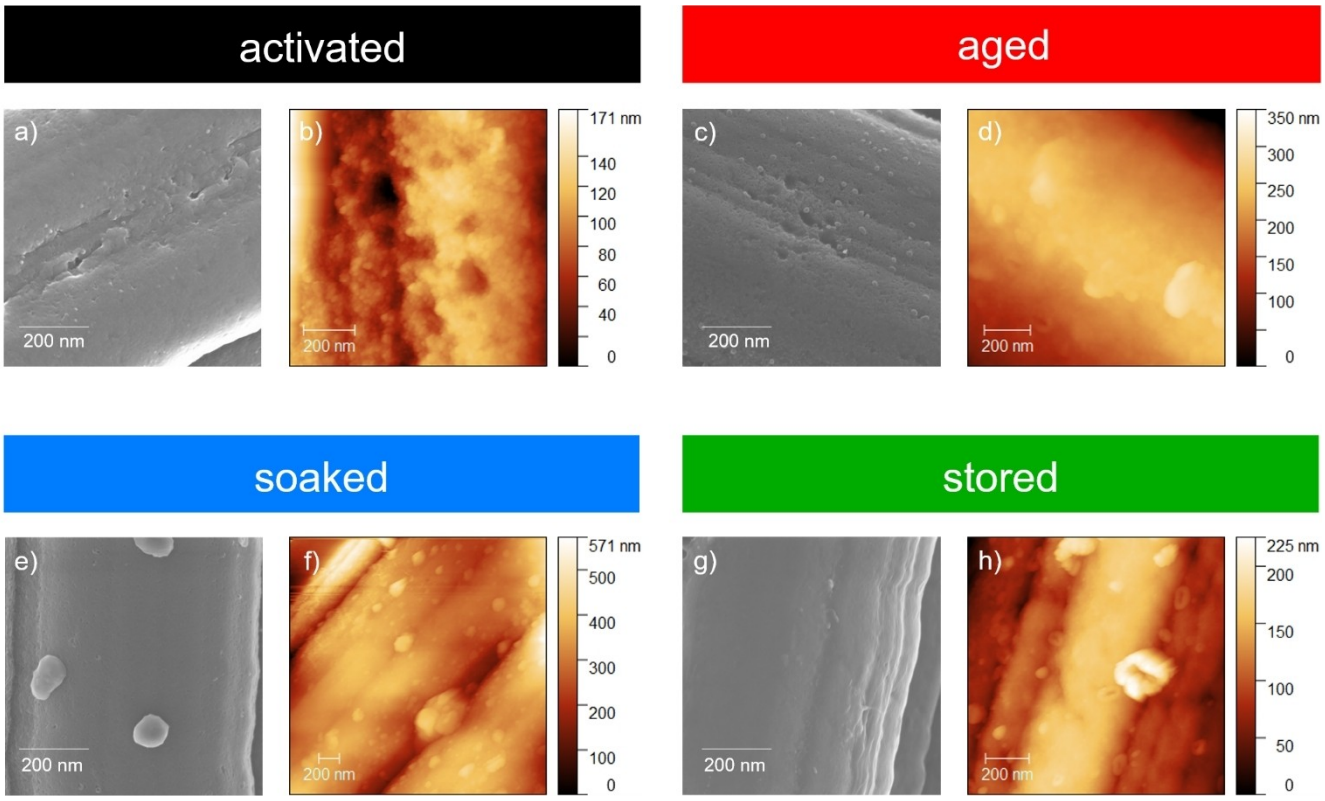

Figure 1. a), c), e), and g) SEM images and b), d), f), and h) AFM height images recorded in peak force tapping mode of differently treated carbon fibers from carbon felts (please note the different z scales in AFM images).

Synchrotron X-Ray Imaging

High electrode saturation is crucial for achieving excellent VFRB performance since only the wetted surface area contributes to the electrochemically active surface area. Here, we use synchrotron X-ray imaging to evaluate the imbibition behavior during injection and after a flow period, mimicking the conditions in a VRFB electrode during operation. Figure 2 displays the saturation of the electrode after the injection process. The carbon felt with different treatments was implemented in a cell setup designed for X-ray imaging.[16,17] The electrolyte was injected into the flow field at the bottom of the measurement cell at a low flow velocity of 0.5 mL min^{-1} to observe the initial imbibition and electrolyte distribution. The electrolyte chose a path through the carbon-based electrode material instead of the flow field. As visible in Figure 2a, the treatment of carbon felts significantly influences the final saturation after the injection process.

The carbon felt, which was only thermally activated, shows a bulk saturation of 90% after the injection. The equally bright part in the center of the respective X-ray radiogram (see Figure 2c) shows that the saturation is constant in the middle of the electrode. The locally resolved saturation calculated for the different sections of the electrode strengthens this finding since the saturation in the center part of the electrode is uniform between 80% and 92% (see Figure 2b). At the flow field side, the saturation is significantly lower since the parts of the electrode next to the flow field remain unfilled (black parts; see Figure 2c). The electrolyte invades the electrode material via the so-called 'highway'-channels and does not spread over the whole material. A broader black stripe is visible on the left side of the X-ray radiogram of the activated carbon felt. Therefore, the calculated saturation at relative thicknesses of more than 85% is decreased. The membrane is located in the X-ray image in this area since it is slightly shifted to the WE side. As visible in Figure 2c, a small part in the middle of the electrode is not fully flooded. The GFA 6.0 EA carbon felt from SGL Carbon is fabricated from two carbon felts combined with a seam. Especially the part near the seam, at around 40% to 45% relative thickness, shows a higher number of unfilled spots. However, the local saturation displayed in Figure 2 was calculated for the whole electrode slice, and the average value does not reflect the locally resolved small bubbles. Previous publications of our group highlight the impact of this manufacturing feature on the imbibition process and flow behavior through the electrode.[15–17]

The artificially aged carbon felt has a bulk saturation of 85% (see Figure 2a). Like the thermally activated sample, the locally resolved saturation of the aged felt is constant at around 80% to 86% in the bulk region. Again, small areas are not thoroughly wetted and remain as black or dark grey spots in the respective X-ray image (see Figure 2d). The area close to the membrane is mainly flooded, but more prominent spots near the flow field remain unfilled compared to the activated sample. This

© 2023 The Authors. ChemSusChem published by Wiley-VCH GmbH

1864564x, 2024, 1, Downloaded from https://chemistry-europe.onlinelibrary.wiley.com/doi/10.1002/cssc.202301063, Wiley Online Library on [01/08/2024]. See the Terms and Conditions (https://onlinelibrary.wiley.com/terms-and-conditions) on Wiley Online Library for rules of use; OA articles are governed by the applicable Creative Commons License

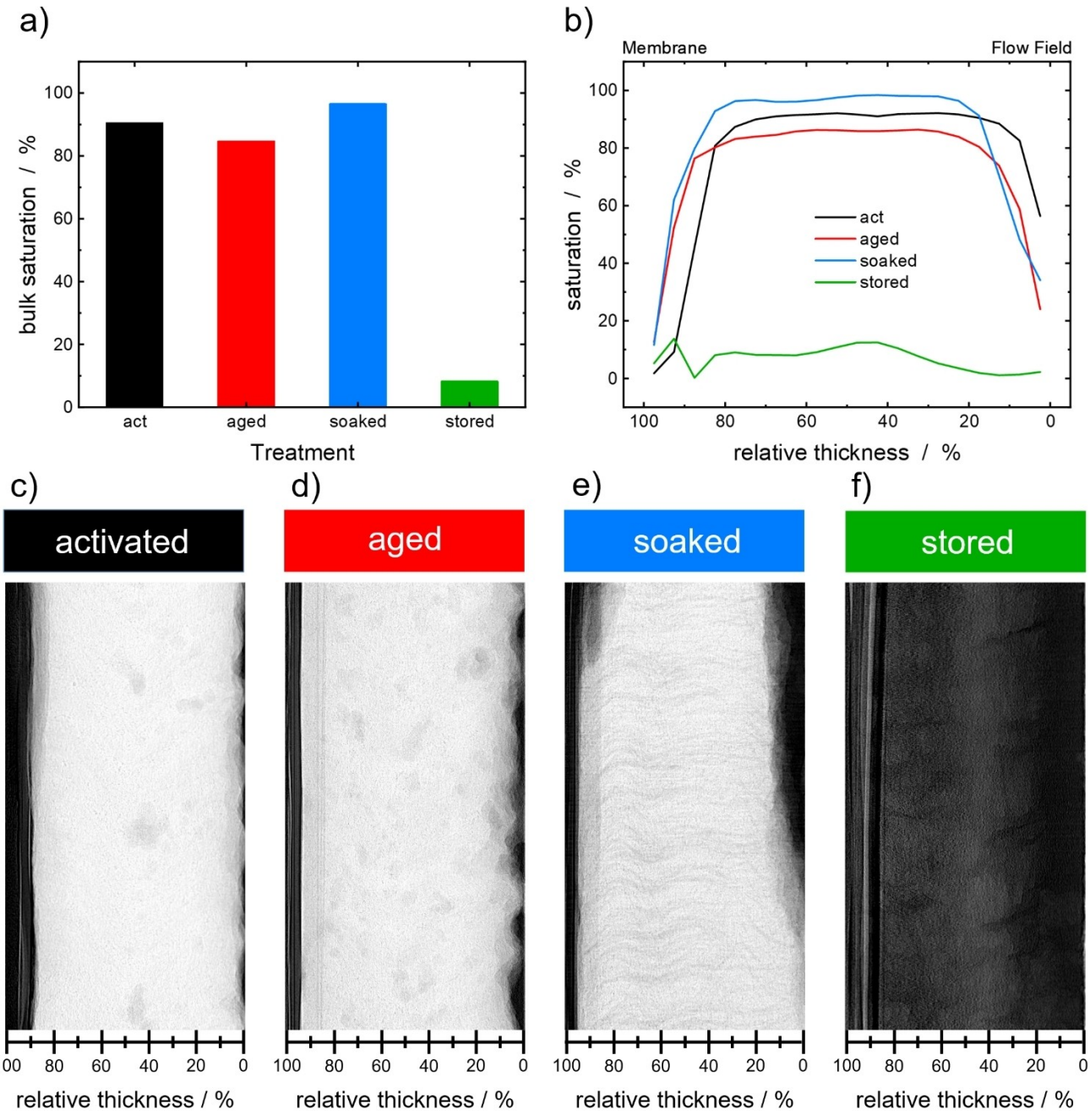

Figure 2. After electrolyte injection into the differently treated carbon felts: a) bulk saturation calculated in the range from 15% to 85% relative thickness, b) locally resolved saturation, and X-ray radiograms of the electrolyte after the injection into c) activated, d) aged, e) soaked, and f) stored carbon felt.

observation shows that the electrolyte imbibition is even more hindered for an aged electrode than for a freshly activated one.

The carbon felt soaked in sulfuric acid displays the highest bulk saturation of all characterized samples, with 96% (Figure 2a).

Nevertheless, the areas outside the bulk, close to the flow field (below 20% relative thickness) and the membrane (above 80% relative thickness), are not entirely saturated. This result shows that the electrolyte imbibition proceeds well in the electrode center, but the lateral spreading is significantly hindered. The whole X-ray image (Figure 2e) displays a wave-like pattern in the electrolyte distribution. Since these features are already visible in the raw image of the electrode before imbibition, they can be assigned to the fiber structure within the electrode, which seems to be followed by the electrolyte during the injection. A higher saturation than the activated carbon felt could be possible due to functionalizing the surface with oxygen-containing groups by soaking the material in an oxidizing acid solution.

The carbon felt, which was thermally activated and then stored in the cabinet for several months, showed an undesirable injection behavior. The bulk saturation after the injection stays

© 2023 The Authors. ChemSusChem published by Wiley-VCH GmbH

1864564x, 2024, 1, Downloaded from https://chemistry-europe.onlinelibrary.wiley.com/doi/10.1002/cssc.202301063, Wiley Online Library on [01/08/2024]. See the Terms and Conditions (https://onlinelibrary.wiley.com/terms-and-conditions) on Wiley Online Library for rules of use; OA articles are governed by the applicable Creative Commons License

low at around 8%, and the area near the flow field remains almost dry. In the region close to the seam (at around 40% relative thickness), some electrolyte was able to invade the electrode material (see Figures 2b and f). However, the maximum electrolyte saturation is only 12%, which indicates that storage of the thermally activated electrode material impedes the electrolyte imbibition.

Therefore, the electrodes should be recently activated before the operation to ensure good performance.

After the injection, the vanadium(IV) electrolyte was pumped through the electrode for 1 minute at 30 mL min^{-1}. Again, the bulk saturation and the locally resolved saturation were calculated, and the X-ray radiograms of the electrolyte are displayed for the four samples in Figure 3.

A slight increase of the bulk saturation from 90% to 93% was calculated for the thermally activated carbon felt. Significant changes in saturation were noticed in the area close to the flow field and next to the membrane, which was afterward mostly filled with electrolyte. Nevertheless, the spots close to the seam are still not entirely wetted and remain visible as dark spots in the respective X-ray image (see Figure 3c). The investigated carbon felts all have a seem in the middle due to the commercial fabrication process. Above 90% relative thickness, the saturation displays a distinctive drop but increases

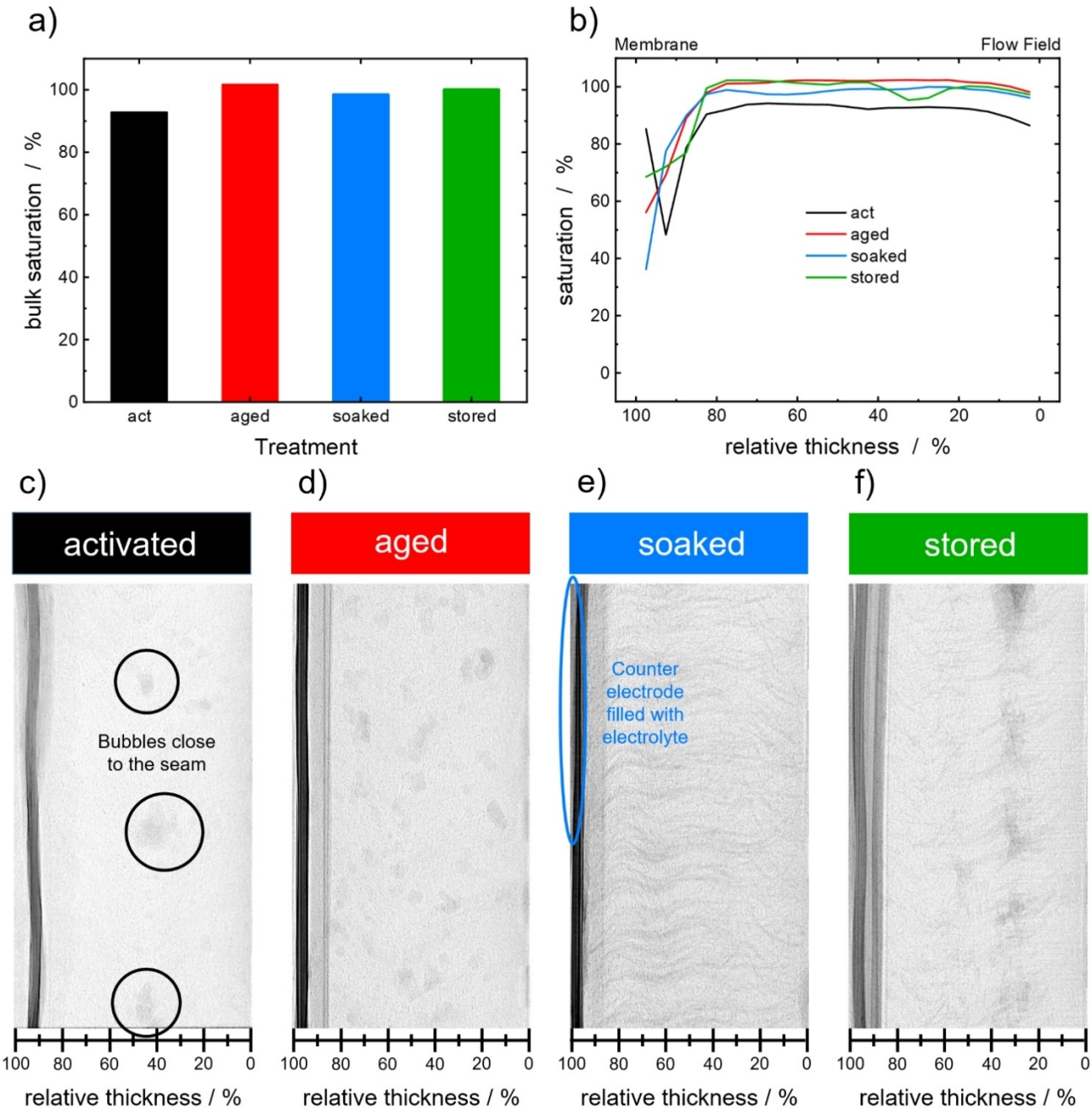

Figure 3. After the flow period through the differently treated carbon felts: a) bulk saturation calculated in the range from 15% to 85% relative thickness, b) locally resolved saturation, and X-ray radiograms of the electrolyte after the flow-through of c) activated, d) aged, e) soaked, and f) stored carbon felt.

© 2023 The Authors. ChemSusChem published by Wiley-VCH GmbH

1864564x, 2024, 1, Downloaded from https://chemistry-europe.onlinelibrary.wiley.com/doi/10.1002/cssc.202301063, Wiley Online Library on [01/08/2024]. See the Terms and Conditions (https://onlinelibrary.wiley.com/terms-and-conditions) on Wiley Online Library for rules of use; OA articles are governed by the applicable Creative Commons License

again at a higher relative thickness. In the X-ray image, this drop is visible as a black stripe corresponding to the membrane separating the carbon felt of interest from the other carbon felt in the cell, which serves as the counter electrode and is not investigated (Figure 3e, left side of image, the carbon felt of the counter electrode filled with electrolyte is highlighted in the image). Since the electrolyte was pumped for one minute at a high flow rate of 30 mL min^{-1}, the electrolyte passed the carbon felt of interest, the tubing, and the other electrode, leading to increased saturation on the left side of the membrane. This feature is not visible for the other investigated samples (see Figures 3d to f) since each cell altered the membrane position differently due to its flexibility.

After the flow period, the activated carbon felt shows the lowest bulk saturation while the aged carbon felt has the highest. This saturation value is slightly over 100% (specifically: 102%) which might be caused by several assumptions necessary for the calculation. Herein, the calculations are based on the Beer-Lambert law adapted by Ge et al.[23] to analyze X-ray absorption images. Previous studies from our group adopted this analysis method for VRFB-based X-ray synchrotron imaging to calculate the electrolyte saturation.[15–17] However, some limitations to the Bert-Lambeer law-based analysis method remain: a uniform sample with a uniform porosity and compression is assumed, the porosity of the pristine sample is used for all samples, slight changes in the electrode arrangement cannot be compensated, and the same beam decay is assumed throughout the whole field of view. Therefore, slight deviations in the electrode's structure, porosity, or compression can cause minor deviations in the saturation analysis, resulting in a value above 100%. Still, this significant increase in electrolyte saturation shows that higher flow velocities were necessary for the aged carbon felt to overcome the higher entry pressures of the areas unfilled after the injection. Some unfilled spots, such as the one in the upper right corner (see Figure 3d), remain in the electrode, showing that the electrolyte prefers already wetted areas as pathways. After this, the less preferred spots are filled. This order of filling the electrode fits our findings from previous publications.[16,17]

The soaked carbon felt sample is similar to the aged sample, with the previously unfilled areas close to the flow field and membrane being filled further (see Figure 3e). Since the bulk saturation was already very high (96%) after the injection, a further electrolyte flow increased the bulk saturation only slightly to 99%.

The most significant changes after the flow period are observed in the stored carbon felt X-ray image. The electrolyte could finally wet the carbon felt, and a high bulk saturation of 100% was reached utilizing high flow rates. The area at around 25% to 35% relative thickness in the electrode's right part remains hydrophobic and unwetted (see Figures 3b and f).

Overall, the saturation after the flow period increased for all samples. Especially at the flow field and the membrane, the electrolyte needs time[17] and a more significant electrolyte flow to overcome the entry pressures and wet the carbon felt. Since commercial flow batteries are operated under constant flow conditions, the original activated felt and the sample after the various treatments are suitable for commercial VRFBs. However, to a fully saturated electrode material, it should be kept in mind that the active species needs to be transported to the active sites. Only wetting a specific spot, which serves later on as dead volume since the used reactant is not flushed away, is not beneficial. Thus, electrodes need good wetting behavior and permeability for the active species.

Further insights into the wettability of the differently treated samples will be gained by dynamic vapor sorption measurements and electrochemical impedance spectroscopy, highlighted in the following sections.

DVS Measurements

High electrode saturation is crucial to achieving an excellent performance of a VRFB. The wettability of the material plays a key role in increasing the active catalytic surface area and reducing pumping losses.

DVS measurements give information about wettability as a bulk property, whereas the synchrotron X-ray experiments deliver more insights into the sample's imbibition behavior, flow behavior, and local electrolyte distribution. These two methods do not probe exactly the same property. Synchrotron X-ray imaging is based on the injection of a liquid in the carbon felt, which fills the voids in the sample. Here, the carbon felt wettability with the liquid can be investigated. In contrast, the DVS measurement characterizes the interaction of the water vapor with the carbon felt surface.

The sorption and desorption isotherms determined from DVS measurements of the differently treated samples are displayed in Figure 4a with a zoom-in on the graph in Figure 4b. The supporting information presents the raw data of the water uptake as a function of time, which is used to determine the isotherms (Figure S1).

All four samples generally show more water uptake at increasing Relative Humidity (RH) and reversible adsorption

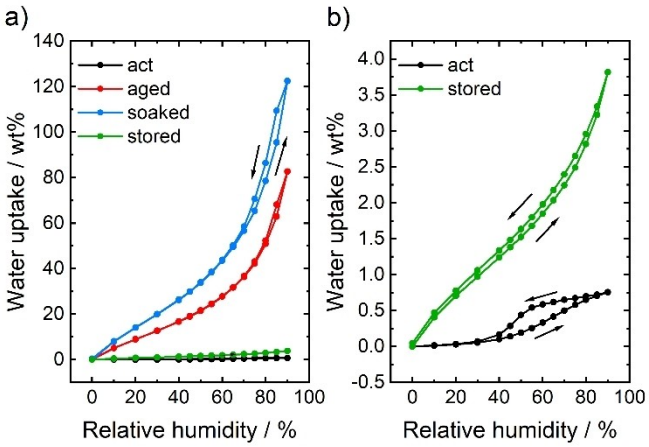

Figure 4. a) Sorption and desorption isotherms of the DVS measurements of treated carbon felts and b) zoom in on the graph displaying only the activated and stored carbon felt.

© 2023 The Authors. ChemSusChem published by Wiley-VCH GmbH

1864564x, 2024, 1, Downloaded from https://chemistry-europe.onlinelibrary.wiley.com/doi/10.1002/cssc.202301063, Wiley Online Library on [01/08/2024]. See the Terms and Conditions (https://onlinelibrary.wiley.com/terms-and-conditions) on Wiley Online Library for rules of use; OA articles are governed by the applicable Creative Commons License

processes. Nevertheless, the shapes of the isotherms and the amount of adsorbed water differ significantly.

As displayed in Figure 4b, the activated carbon felt shows a maximum water uptake of 0.8 wt% at 90% RH and the typical sigmoidal shape of a sorption isotherm of type V caused by relatively weak interactions of adsorbents and adsorbates.[24,25] At low RH, only minimal amounts of water are adsorbed since the water vapor will only interact with the polar functional groups, primarily oxygen-containing groups for carbon-based samples, according to the literature.[25–27] At higher RH, a steep increase is caused by strong interactions of adsorbed water molecules and water vapor leading to the formation of multimolecular layers and pore filling.[24,28] During desorption, a significant hysteresis loop is visible, which displays features of the H2 type and is caused by capillary condensation due to strong hydrogen bond interactions of water molecules and pore blocking due to the sample's porous structure.[24,26,29]

The other samples display a different isotherm shape and significantly higher water uptake. The stored carbon felt exhibits a slightly enhanced maximum water uptake of 3.8 wt% at 90% RH Whereas, the aged and the soaked carbon felt take up significantly larger amounts of water, with 122.5 wt% and 82.7 wt%, respectively. The water uptake values could be higher since an equilibrium weight is not reached above 80% RH for the aged and soaked carbon felt (see supporting information). The isotherms show an ogee shape and only minimal hysteresis, fitting isotherm type II.[24,28] The water adsorption starts at low RH values due to many active polar sites on the material's surface. Due to a significant overlap of monolayer and multilayer adsorption, no clear monolayer coverage can be determined, and the graph has a steep slope at high RH. The stored sample was exposed to the air in a cabinet for several months. During this time, carbon surface oxidation can occur due to atmospheric oxygen. Thus, more polar functional groups are present at the carbon felt's surface, and more water can be adsorbed. Surprisingly, this sample shows a higher water uptake than the activated carbon felt since the synchrotron X-ray experiments presented above and the following EIS results would imply a lower wettability for the stored sample. However, this discrepancy could be caused by a different wetting behavior of the liquid electrolyte and the water vapor.

The aged and soaked samples are treated with chemicals during the artificial aging in vanadium- and sulfuric acid-containing electrolyte or the soaking process in diluted sulfuric acid. The contact with these chemicals leads to surface oxidation and introduces polar functional groups.[27] Especially the presence of sulfuric acid, known as an oxidizing acid, seems to influence the abundance of active sites significantly.

All samples with isotherms of type II (aged, soaked, and stored carbon felt) show minimal hysteresis. Since the surfaces are roughened, a different pore structure is introduced, and more active sites could be easily accessible without such effects as capillary condensation or pore blocking.[24,28,29]

EIS and DRT Analysis

In addition to synchrotron X-ray imaging and the DVS measurements, EIS provides an additional way to characterize the wettability of carbon materials. In a recent publication of our group, we were able to assign the peaks in the DRT spectrum to physical processes, namely the electrochemical reaction in the high frequency (HF) range, the transport processes in the medium frequency (MF) range, and the ion transport in the low frequency (LF) range.[19] Furthermore, we demonstrated that carbon felts' wettability and surface morphology are linked using DVS and EIS coupled with DRT analysis.[20]

Here, EIS measurements of the carbon felt with different treatments were performed at 1.05 V vs. RHE in vanadium(IV) electrolyte. The electrolyte was pumped constantly through the carbon material to mimic the conditions in a commercial VRFB during the EIS measurement and ensure steady-state conditions required for reliable data acquisition. Figure 5a displays the Nyquist plots of the carbon felts exposed to different treatment processes. The DRT method was used to separate the individual contributions of the processes (see Figure 5b). In the high-frequency range (above 250 Hz), one single peak is observed corresponding to the electrochemical reaction.[19] This peak shifts slightly with different treatments since the surface is altered, affecting the catalytic activity. Below 20 mHz (low-frequency range), the single peak corresponds to the ion transport through the electrolyte. The impedance related to this process differs significantly for the materials. The previous synchrotron X-ray experiments and DVS measurements indicated different wettability, supported by these EIS results. In the mid-frequency range, several visible peaks are assigned to the transport through the porous structure of the electrolyte. Here, the related impedance is strongly dependent on the material's treatment.

Figure 5c displays the absolute values of the three processes to highlight the large deviation between the materials. The activated carbon sample exhibits a relatively low overall cell impedance (the combination of the LF, MF, and HF contributions). The impedance of the HF process is around half of the other HF impedances of the samples, and the activated carbon felt shows the best behavior in the cyclic voltammetry study on the positive side (see next chapter, Figure 6a). Altering the surface by treatments leads to higher HF impedances and, thus, to a weaker electrochemical performance. Figure 5d shows the relative contributions of the impedance contributions. For the activated sample, the main contribution is the LF process. The aged carbon felt has the lowest overall impedance of all characterized carbon felts. The absolute value of the MF impedances is the same for the activated and aged carbon felt. However, the LF impedance is decreased, implying that the ion transport is less hindered due to the higher wettability of the material (see DVS results). The soaked carbon felt exhibited a larger impedance than the activated and aged sample. The MF and LF impedances are increased compared to these samples and contribute almost equally to the overall impedance. As clearly visible in the Nyquist plot (see Figure 5a), the stored carbon felt exhibits the largest overall impedance, mainly

© 2023 The Authors. ChemSusChem published by Wiley-VCH GmbH

1864564x, 2024, 1, Downloaded from https://chemistry-europe.onlinelibrary.wiley.com/doi/10.1002/cssc.202301063, Wiley Online Library on [01/08/2024]. See the Terms and Conditions (https://onlinelibrary.wiley.com/terms-and-conditions) on Wiley Online Library for rules of use; OA articles are governed by the applicable Creative Commons License

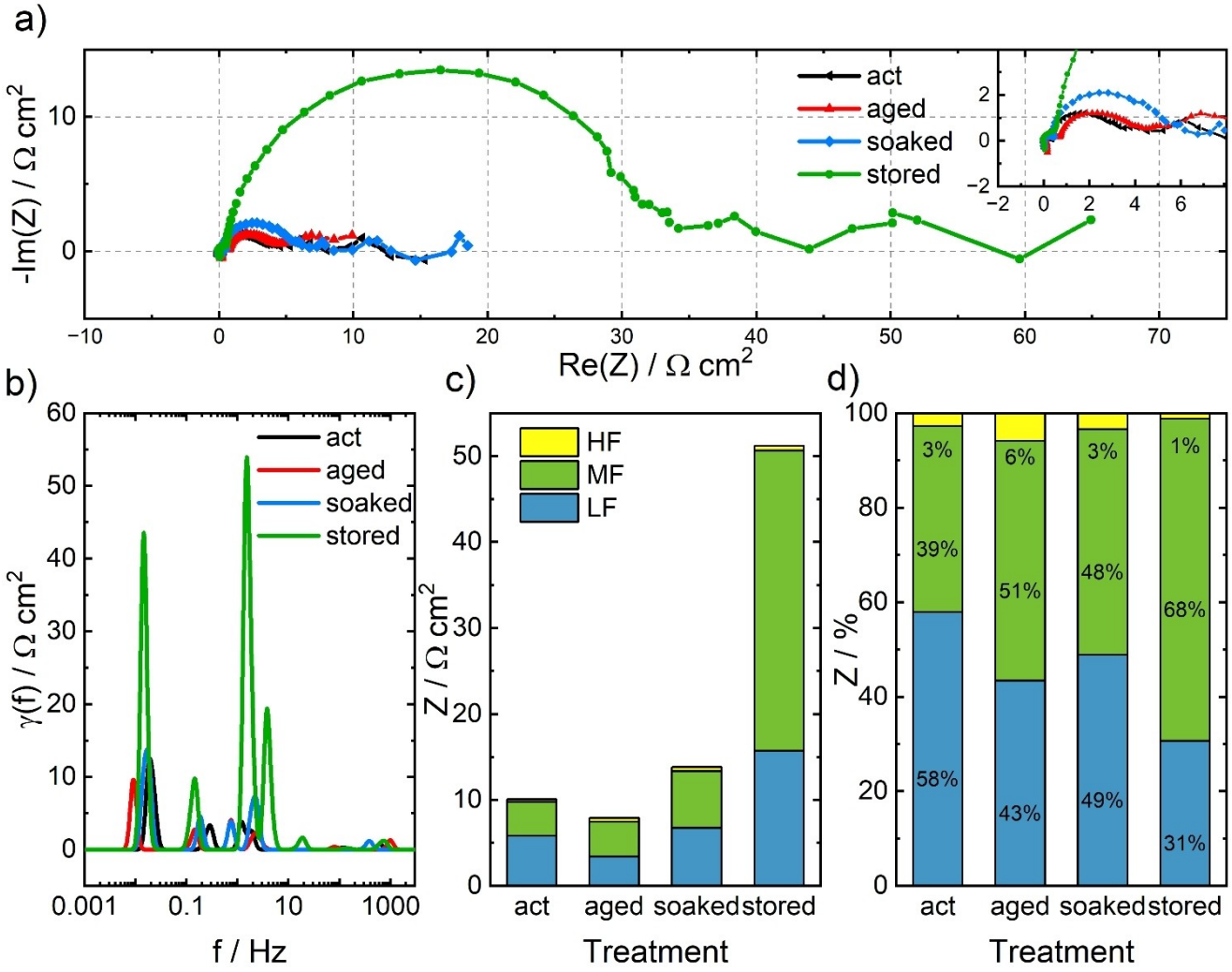

Figure 5. a) Nyquist plot of the differently treated carbon felts based on an EIS measurement performed at 1.05 V vs. RHE at constant electrolyte flow including zoom-in on graph; b) corresponding DRT spectra, c) absolute impedances and d) relative impedance contributions of the LF, MF, and HF processes determined from the DRT spectra.

caused by the high values of MF and LF impedances. The synchrotron X-ray experiments highlighted that the electrolyte injection into the stored felt is rugged, which is supported by the EIS and DRT results showing increased impedances for the transport-related processes.

Cyclic Voltammetry

In addition to the EIS experiments, CV studies were performed to characterize the electrochemical performance of the differently treated carbon felts in the positive half-cell (see Figure 6) and the negative half-cell (see Figure 7). The CVs are displayed in Figure 6a and Figure 7a, the peak-to-peak separations of anodic and cathodic peak ΔE in b, and the charge ratio $C_{anodic}/C_{cathodic}$ in c. The authors focused on evaluating the electrochemical performance in the half-cell measurements to assess the performance of treated electrodes in detail and correlate observed changes to specific electrode properties. This allows us to separate individual effects caused by the treatments and even resolve the contributions for both half-cells. Additional components in the full cell, such as the membrane, would add new variables to the system, which might obscure a detailed analysis.

The potential range of the vanadium(IV)/vanadium(V) reaction was chosen to study the performance of the carbon felt on the positive half-cell. Figure 6a reveals similar shapes of the CVs for all samples except the cathodic scan of the stored carbon felt. The CVs of activated, aged, and soaked carbon felts display similar peak shapes for the anodic and cathodic scans and high charge ratios of 94%, 91%, and 95%, respectively (see Figure 6c). Thus, these samples show good vanadium(IV)/vanadium(V) reaction reversibility. However, the stored carbon felt has a significantly lower maximum current during the cathodic scan than the anodic scan and the cathodic peak is significantly broader. At the same time, the charge ratio is significantly decreased to 81%. Since the stored sample has the highest HF impedance, which is correlated to the electro-

© 2023 The Authors. ChemSusChem published by Wiley-VCH GmbH

1864564x, 2024, 1, Downloaded from https://chemistry-europe.onlinelibrary.wiley.com/doi/10.1002/cssc.202301063, Wiley Online Library on [01/08/2024]. See the Terms and Conditions (https://onlinelibrary.wiley.com/terms-and-conditions) on Wiley Online Library for rules of use; OA articles are governed by the applicable Creative Commons License

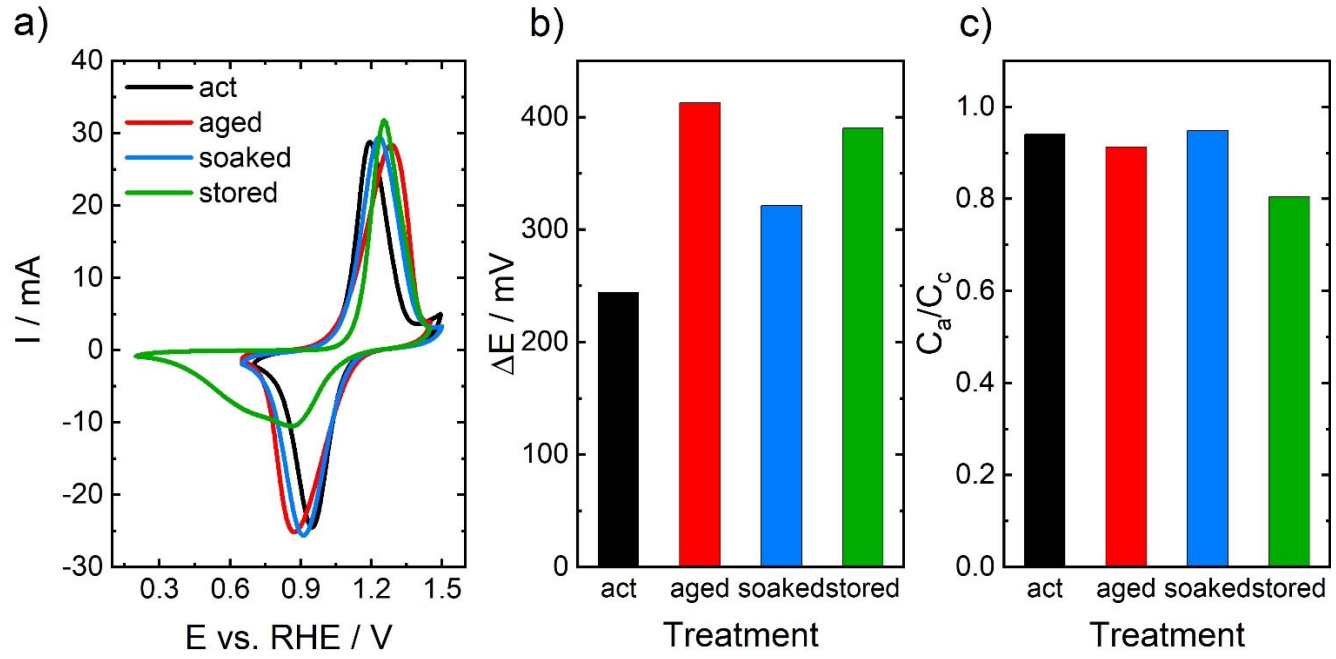

Figure 6. CV measurements of differently treated carbon felts in 0.1 M VO^{2+} in 2 M H_2SO_4 at a scan rate of 2 mV s^{-1} (positive half-cell); b) peak-to-peak separations ΔE, and c) charge ratios $C_{cathodic}/C_{anodic}$ determined from the CVs shown in a).

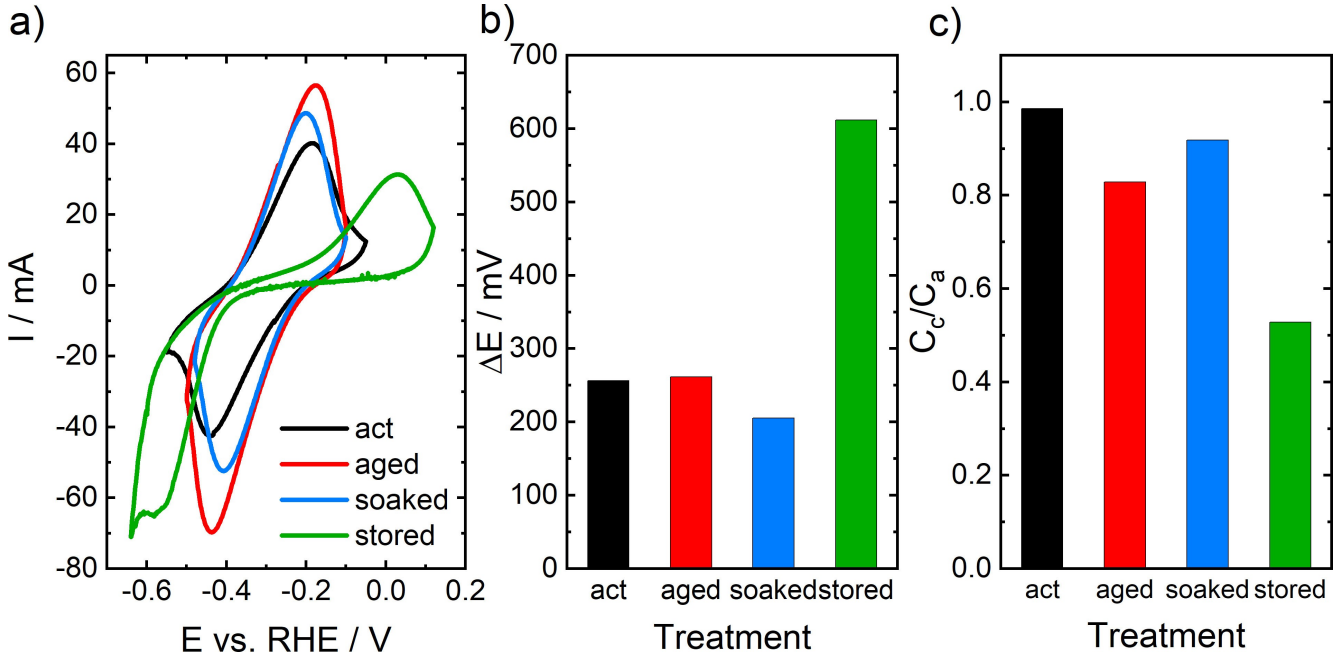

Figure 7. CV measurements of differently treated carbon felts in 0.1 M V^{2+} in 2 M H_2SO_4 at a scan rate of 2 mV s^{-1} (negative half-cell); b) peak-to-peak separations ΔE, and c) charge ratios $C_{anodic}/C_{cathodic}$ determined from the CVs shown in a).

chemical reaction, the CV results follow the trends of the EIS measurements. The reduction reaction is slower and considerably more sluggish.

The peak-to-peak separations ΔE of the treated carbon samples are also investigated to study the reversibility of the redox reaction (see Figure 6b). The activated carbon felt shows the lowest ΔE with 244 mV, which is quite far from the theoretical value of a reversible one-electron transfer reaction.[30] The aged and stored carbon felts show the largest ΔE of 413 mV and 390 mV, respectively. Since their charge ratios are also decreased to 91 % and 81 %, the electrochemical performance of the carbon felt and the reaction reversibility decreases with the material's aging and storing.

Additionally, the chemical reactions occurring in the negative half-cell, the oxidation and reduction of vanadium(II)/vanadium(III), were investigated, and the CVs are displayed in

© 2023 The Authors. ChemSusChem published by Wiley-VCH GmbH

1864564x, 2024, 1, Downloaded from https://chemistry-europe.onlinelibrary.wiley.com/doi/10.1002/cssc.202301063, Wiley Online Library on [01/08/2024]. See the Terms and Conditions (https://onlinelibrary.wiley.com/terms-and-conditions) on Wiley Online Library for rules of use; OA articles are governed by the applicable Creative Commons License

Figure 7a. The activated, aged, and soaked samples show similar shapes in the CV during the anodic and cathodic scans. Again, the CV of the stored carbon felt differs significantly from these measurements. The ΔE of the stored sample is very high (612 mV) since the oxidation reaction is shifted to higher potentials and the reduction reaction to more negative potentials due to the sluggish kinetics of the reaction at this material. Compared to all other samples, the onset of HER is visible at around −0.6 V vs. RHE since the potential range of the vanadium reactions overlaps significantly with the potential range of the HER. The measured current signal is noisy, and a steep decay is monitored at potentials smaller than −0.6 V vs. RHE. These measurements confirmed our previous study using differential electrochemical mass spectroscopy that the desired vanadium reaction and the undesired HER occur at these potentials.[6,7] Since the undesired reaction reduces the number of electrons for the vanadium(III) reduction reaction, preventing the HER is key for high efficiency. Here, a charge ratio $C_{cathodic}/C_{anodic}$ of 53% is calculated for the stored carbon felt, indicating that a large share of the cathodic current can be attributed to the HER.

In contrast, the activated carbon felt has an almost ideal charge ratio of 99% and a ΔE of 256 mV, indicating that almost no HER is taking place in the measured potential range. Nevertheless, the maximum currents during anodic and cathodic scans are smaller than the aged and the soaked samples, with 83% and 92% charge ratio, respectively. Since the aged and the soaked sample got in contact with oxidizing chemicals during the sample preparation, the surface is roughened, and more electrochemically active surface area is available, leading to higher currents.[27]

In summary, the activated carbon felt shows a good electrochemical performance in the positive and the negative half-cell. Compared to this sample, the artificial aging process causes losses in performance due to a decreased charge ratio. The stored sample exhibited the lowest performance in both half-cells, demonstrating that the carbon felt should be implemented in the VRFB cell directly after the thermal activation.

Conclusions

In this study, we investigated the effects of different treatments on a carbon felt electrode material using several characterization techniques. The investigations deepen the understanding of the challenges in long-term use of VRFB electrodes. To mimic these typical electrode degradations, four types of carbon felts were investigated: a thermally activated carbon felt that was artificially aged, one soaked in sulfuric acid, and the last stored in a cabinet.

During the synchrotron X-ray experiments, the electrolyte injection led to a high electrolyte saturation in the activated, aged, and soaked samples, whereas the stored carbon felt was almost not invaded. Nevertheless, after a flow period at a higher flow rate, even the stored carbon felt reached a high saturation since the electrolyte is forced into the material. Since commercial VRFBs are used under constant electrolyte flow, these observations show that all materials are suitable for VRFB operation, but some might need higher pumping velocities to ensure sufficient electrode wetting in the beginning. The treatment of the carbon material influences this significantly. However, the electrode material must be wetted, and the active sites must also be provided with active species during the operation.

The bulk wettability of the treated carbon felts was investigated by DVS, and significant differences in water uptake were determined. The samples, which were in contact with sulfuric acid during the treatment, showed a drastically enhanced water uptake. Furthermore, the morphology changes after the different treatments were investigated using AFM and SEM. These techniques revealed that different treatments impact the electrode structure, which influences the surface wettability of the electrode materials due to different nano-sized structural features and functional groups at the surface.

To deepen the understanding of the processes in the electrode materials, EIS was combined with DRT analysis and revealed that the treatment influences the impedance related to the electrochemical reaction due to changes in the active sites on the surface. The effects for the transport-related processes follow the same trends observed in the synchrotron X-ray imaging experiments and the DVS measurements exhibiting increased transport impedances for less wettable materials.

Furthermore, the electrochemical performance was studied by CV. The best positive and negative half-cell performance was observed for the activated carbon felt, displaying a low peak-to-peak separation and high reversibility. Storing the carbon felt decreases the catalytic activity and the reaction reversibility of the carbon felt significantly, whereas soaking and aging only slightly altered the electrochemical performance demonstrating the suitability of carbon felts for VRFBs.

These investigations are crucial to understanding the effects of the different degradation processes in carbon felts on the performance and optimizing the carbon materials for VRFBs.

Experimental Section

Materials and Electrolytes

A scheme highlighting the preparation of the carbon felts is presented in the supporting information (Figure S2). SGL Carbon (Meitingen, Germany) supplied the carbon felt SIGRACELL® GFA 6.0 EA, which was thermally pretreated as proposed in the literature to enhance the wettability and the electrochemical performance.[4,5] The carbon felt was placed in a covered glass petri dish and heated to 400 °C for 25 h in a muffle furnace in an air atmosphere. The sample is referred to as activated carbon felt in the following.

For the aging treatment resulting in the aged carbon felt, we applied a potential of 1.2 V vs. RHE to the thermally activated carbon felt in 0.1 M VO_2^+ in 2 M sulfuric acid for 5 days. This treatment represents electrochemical aging.

The soaked carbon felt sample was prepared by soaking an activated carbon felt in 4 M sulfuric acid for 15 days at 40 °C. Here, the chemical aging of the carbon felt was mimicked.

© 2023 The Authors. ChemSusChem published by Wiley-VCH GmbH

1864564x, 2024, 1, Downloaded from https://chemistry-europe.onlinelibrary.wiley.com/doi/10.1002/cssc.202301063, Wiley Online Library on [01/08/2024]. See the Terms and Conditions (https://onlinelibrary.wiley.com/terms-and-conditions) on Wiley Online Library for rules of use; OA articles are governed by the applicable Creative Commons License

The stored carbon felt was solely activated according to the activation process described above and stored in a bag at room temperature in air for several months. This step imitates the time-dependent aging process.

Vanadium(IV) electrolyte (0.1 M $VOSO_4$ in 2 M H_2SO_4) was prepared by dissolving $VOSO_4$ (vanadyl sulfate hydrate, 99.9% metal basis, Thermo Fisher Scientific) in diluted H_2SO_4 (diluted from concentrated sulfuric acid, 96%, Suprapur®, Merck with ultrapure water (18.2 MΩ cm)). This electrolyte was used for the electrochemical measurements with the positive half-cell setup and the synchrotron X-ray imaging experiments.

A charging procedure was performed to transfer vanadium(IV) into vanadium(II) electrolyte using a VRFB in a redox flow test system (Scribner 857 Redox Flow Cell Test System, Scribner Associates Inc.). The charged electrolyte was utilized to electrochemically characterize the vanadium(II)/vanadium(III) half-cell reaction.

Surface Imaging: SEM and AFM

The materials' structure and morphology were investigated using SEM and AFM. The SEM images were conducted with an LEO 1550 VP (Carl Zeiss AG, InLens detector, 3 keV acceleration voltage).

For the AFM imaging, single carbon fibers were extracted from the carbon felt and glued to a Menzel microscopy glass, utilizing PELCO carbon tabs. The single carbon fibers were characterized with a Dimension Icon instrument (Bruker Corporation) using a ScanAsyst-Air probe with approximately 2 nm tip radius and 15° broadening. The images were recorded in Quantitative Nanomechanical Mapping mode, displaying the height sensor output. The program Gwyddion 2.62[31] was used for the subsequent line scan analysis, during which a zero correction was applied to set the zero point. The displayed images were further post-processed by polynomial background correction of first order to remove the fiber bending and increase the visibility of more minor features in the images.

Electrochemical Characterization

The electrochemical performance of the samples was evaluated with CV and EIS measurements. All measurements were performed in a three-electrode setup with an in-house developed flow cell[19] and an SP-300 potentiostat (BioLogic Science Instruments). The carbon felts were cut into rectangular pieces (1.0 cm×1.0 cm) and placed in the flow cell. The WE was contacted by a gold foil (0.25 mm, 99.9975 + %, Alfa Aesar) and a gold wire (Ø 0.5 mm, 99.9975 + %, Alfa Aesar) when measuring in the potential range of the vanadium(IV)/(vanadium(V) reaction (positive half-cell setup). The contacts were changed to a titanium foil (1.0 mm, 99.2%, Alfa Aesar) and a titanium wire (0.28 mm, Alfa Aesar) when studying the vanadium(II)/vanadium(III) reaction (negative half-cell setup) since gold is known to catalyze the HER at these negative potentials.[32]

All experiments used an in-house developed hydrogen reference electrode as the RE and a thermally activated carbon felt (2.5 cm×2.5 cm) as the CE The carbon felt was contacted with a titanium foil and a gold wire (positive half-cell setup) or a titanium plate and titanium wire (negative half-cell setup). The CVs were conducted at room temperature with a scan rate of 2 mV s^{-1} while no flow was applied. Potential limits were chosen to make the peaks from anodic and cathodic scans completely visible.

EIS was utilized to analyze the electrode processes in the positive half-cell using the setup for the positive half-cell described above. The EIS measurements were performed at room temperature at a flow rate of 15 mL min^{-1} in the potentiostatic mode in a frequency range from 100 kHz to 3.5 mHz with a single sinusoidal excitation of 5 mV as the perturbation and an applied potential of 1.05 V vs. RHE. The measurement is started after an equilibration phase of 5 minutes at 1.05 V vs. RHE. During the measurements, the electrolyte was pumped from the electrolyte reservoir through the flow cell and back to the reservoir by a peristaltic pump (Masterflex L/S®, Cole-Parmer). Continuous pumping is required to ensure steady-state conditions necessary to gain meaningful impedance data.

The data were further analyzed using a MATLAB-based tool called DRTtools[33] based on the Tikhonov regularization. The spectra fitting is based on a Gaussian function for the discretization and includes the inductive data.

DVS

DVS measurements were performed with a Q5000 Sorption Analyzer (TA Instruments). At the measurement's beginning and end, the sample is heated up to 60 °C for 240 min to remove water residues. Sorption and desorption isotherms under nitrogen gas flow at 25 °C are measured between 0% and 90% RH. The RH was changed stepwise by 10% from 0% to 40% RH and in 5% intervals at higher RHs to ensure enough data points. The measurement time at each step was adapted for different RHs to reach a mass equilibrium after each sorption/desorption step. At 50% RH and below, the RH remained constant for 90 min. Between 55% and 75%, the time was increased to 120 min. For the highest RHs, the measurement time was set to 180 min for 80% and 85% RH and to 240 min for 90% RH.

Synchrotron X-Ray Imaging

The X-ray radiograms were captured at the Biomedical Imaging and Therapy Bending Magnet (BMIT-ID) 05ID-2 beamline at the Canadian Light Source Inc. (Saskatoon, Saskatchewan, Canada), using the identical settings and setup as in our previous publications.[16,17] The details regarding the experimental setup, the settings, and the data evaluation can be found in the supporting information (Figure S3) and in the mentioned publications.

This study compressed the electrode by 25%, and an interdigitated flow field for flow-by configuration was used. During the experiment, the electrolyte was first injected into the carbon felts at 0.5 mL min^{-1} for 5 min (injection process). Second, the electrolyte was pumped through the electrode material at 30 mL min^{-1} for 1 min (flow process).

The recorded radiograms were post-processed and analyzed according to previous publications.[15–17]

Acknowledgements

We especially thank SGL Carbon for supplying the SIGRACELL® carbon felt. MS and KK gratefully acknowledge financial support through a Kekulé Ph.D. fellowship by the Fonds der Chemischen Industrie (FCI). The authors also gratefully acknowledge funding support from the Natural Sciences and Engineering Research Council of Canada (NSERC) Discovery Grant Program and the Canada Research Chairs Program. This study was further supported by Sergey Gasilov, Denise Miller, Adam Webb, Ning Zhu, and the Biomedical Imaging and Therapy (BMIT) beamline staff. The research described in this paper was performed at the Canadian Light Source, which is supported by the Canada

© 2023 The Authors. ChemSusChem published by Wiley-VCH GmbH

1864564x, 2024, 1, Downloaded from https://chemistry-europe.onlinelibrary.wiley.com/doi/10.1002/cssc.202301063, Wiley Online Library on [01/08/2024]. See the Terms and Conditions (https://onlinelibrary.wiley.com/terms-and-conditions) on Wiley Online Library for rules of use; OA articles are governed by the applicable Creative Commons License

Foundation for Innovation, Natural Sciences and Engineering Research Council of Canada, the University of Saskatchewan, the Government of Saskatchewan, Western Economic Diversification Canada, the National Research Council Canada, and the Canadian Institutes of Health Research. This work contributes to the research performed at CELEST (Center for Electrochemical Energy Storage Ulm-Karlsruhe). MJ thanks the Research Training group "Confinement-controlled Chemistry", which is funded by the Deutsche Forschungsgemeinschaft (DFG, German Research Foundation)-GRK2376/331085229. Additionally, the authors thank Bruker Germany and in particular Bruker Nano GmbH for letting us use their AFM facilities. Open Access funding enabled and organized by Projekt DEAL.

Conflict of Interests

The authors declare no conflict of interest.

Data Availability Statement

The data that support the findings of this study are available from the corresponding author upon reasonable request.

Keywords: Carbon · Electrochemical impedance spectroscopy and distribution of relaxation times analysis · Synchrotron X-ray imaging · Vanadium · Wettability

[1] K. Lourenssen, J. Williams, F. Ahmadpour, R. Clemmer, S. Tasnim, *J. Energy Storage* **2019**, *25*, 100844.
[2] K. J. Kim, M.-S. Park, Y.-J. Kim, J. H. Kim, S. X. Dou, M. Skyllas-Kazacos, *J. Mater. Chem. A* **2015**, *3*, 16913–16933.
[3] B. Sun, M. Skyllas-Kazacos, *Electrochim. Acta* **1992**, *37*, 2459–2465.
[4] A. M. Pezeshki, J. T. Clement, G. M. Veith, T. A. Zawodzinski, M. M. Mench, *J. Power Sources* **2015**, *294*, 333–338.
[5] L. Eifert, R. Banerjee, Z. Jusys, R. Zeis, *J. Electrochem. Soc.* **2018**, *165*, A2577–A2586.
[6] L. Eifert, Z. Jusys, R. Banerjee, R. J. Behm, R. Zeis, *ACS Appl. Energ. Mater.* **2018**, *1*, 6714–6718.
[7] L. Eifert, Z. Jusys, R. J. Behm, R. Zeis, *Carbon* **2020**, *158*, 580–587.
[8] D. J. Suárez, Z. González, C. Blanco, M. Granda, R. Menéndez, R. Santamaría, *ChemSusChem* **2014**, *7*, 914–918.
[9] Z. González, A. Sánchez, C. Blanco, M. Granda, R. Menéndez, R. Santamaría, *Electrochem. Commun.* **2011**, *13*, 1379–1382.
[10] R. Schweiss, A. Pritzl, C. Meiser, *J. Electrochem. Soc.* **2016**, *163*, A2089-A2094.
[11] C.-N. Sun, F. M. Delnick, L. Baggetto, G. M. Veith, T. A. Zawodzinski, *J. Power Sources* **2014**, *248*, 560–564.
[12] R. Huang, S. Liu, Z. He, W. Zhu, G. Ye, Y. Su, W. Deng, J. Wang, *Adv. Funct. Mater.* **2022**, *32*, 2111661.
[13] M. Park, J. Ryu, J. Cho, *Chem. Asian J.* **2015**, *10*, 2096–2110.
[14] L. Wei, T. S. Zhao, Q. Xu, X. L. Zhou, Z. H. Zhang, *Appl. Energy* **2017**, *190*, 1112–1118.
[15] N. Bevilacqua, L. Eifert, R. Banerjee, K. Köble, T. Faragó, M. Zuber, A. Bazylak, R. Zeis, *J. Power Sources* **2019**, *439*, 227071.
[16] L. Eifert, N. Bevilacqua, K. Köble, K. Fahy, L. Xiao, M. Li, K. Duan, A. Bazylak, P.-C. Sui, R. Zeis, *ChemSusChem* **2020**, *13*, 3154–3165.
[17] K. Köble, L. Eifert, N. Bevilacqua, K. F. Fahy, A. Bazylak, R. Zeis, *J. Power Sources* **2021**, *492*, 229660.
[18] a) M. Gebhard, M. Schnucklake, A. Hilger, M. Röhe, M. Osenberg, U. Krewer, I. Manke, C. Roth, *Energy Technol.* **2020**, *8*, 1901214; b) R. Jervis, M. D. Kok, T. P. Neville, Q. Meyer, L. D. Brown, F. Iacoviello, J. T. Gostick, D. J. Brett, P. R. Shearing, *J. Energy Chem.* **2018**, *27*, 1353–1361; c) P. Trogadas, O. O. Taiwo, B. Tjaden, T. P. Neville, S. Yun, J. Parrondo, V. Ramani, M.-O. Coppens, D. J. Brett, P. R. Shearing, *Electrochem. Commun.* **2014**, *48*, 155–159; d) D. Emmel, J. D. Hofmann, T. Arlt, I. Manke, G. D. Wehinger, D. Schröder, *ACS Appl. Energ. Mater.* **2020**, *3*, 4384–4393.
[19] M. Schilling, M. Braig, K. Köble, R. Zeis, *Electrochim. Acta* **2022**, *430*, 141058.
[20] K. Köble, M. Jaugstetter, M. Schilling, M. Braig, T. Diemant, K. Tschulik, R. Zeis, *J. Power Sources* **2023**, *569*, 233010.
[21] S. Zhong, C. Padeste, M. Kazacos, M. Skyllas-Kazacos, *J. Power Sources* **1993**, *45*, 29–41.
[22] S. D. Beinlich, N. G. Hörmann, K. Reuter, *ACS Catal.* **2022**, *12*, 6143–6148.
[23] N. Ge, S. Chevalier, J. Hinebaugh, R. Yip, J. Lee, P. Antonacci, T. Kotaka, Y. Tabuchi, A. Bazylak, *J. Synchrotron Radiat.* **2016**, *23*, 590–599.
[24] M. Thommes, K. Kaneko, A. V. Neimark, J. P. Olivier, F. Rodriguez-Reinoso, J. Rouquerol, K. S. Sing, *Pure Appl. Chem.* **2015**, *87*, 1051–1069.
[25] J. J. Mahle, *Carbon* **2002**, *40*, 2753–2759.
[26] L. Liu, S. J. Tan, T. Horikawa, D. D. Do, D. Nicholson, J. Liu, *Adv. Colloid Interface Sci.* **2017**, *250*, 64–78.
[27] J. Choma, W. Burakiewicz-Mortka, M. Jaroniec, Z. Li, J. Klinik, *J. Colloid Interface Sci.* **1999**, *214*, 438–446.
[28] J. Yuan, Q. Chen, B. Fei, *Eur. J. Wood Prod.* **2021**, *79*, 1131–1139.
[29] J. Alcañiz-Monge, A. Linares-Solano, B. Rand, *J. Phys. Chem. B* **2001**, *105*, 7998–8006.
[30] N. Elgrishi, K. J. Rountree, B. D. McCarthy, E. S. Rountree, T. T. Eisenhart, J. L. Dempsey, *J. Chem. Educ.* **2018**, *95*, 197–206.
[31] D. Nečas, P. Klapetek, *Cent. Eur. J. Phys.* **2012**, *10*, 181–188.
[32] J. Perez, E. R. Gonzalez, H. M. Villullas, *J. Phys. Chem. B* **1998**, *102*, 10931–10935.
[33] T. H. Wan, M. Saccoccio, C. Chen, F. Ciucci, *Electrochim. Acta* **2015**, *184*, 483–499.

Manuscript received: July 20, 2023
Revised manuscript received: August 29, 2023
Accepted manuscript online: September 6, 2023
Version of record online: October 30, 2023

© 2023 The Authors. ChemSusChem published by Wiley-VCH GmbH

1864564x, 2024, 1, Downloaded from https://chemistry-europe.onlinelibrary.wiley.com/doi/10.1002/cssc.202301063, Wiley Online Library on [01/08/2024]. See the Terms and Conditions (https://onlinelibrary.wiley.com/terms-and-conditions) on Wiley Online Library for rules of use; OA articles are governed by the applicable Creative Commons License